PURE-LET DECONVOLUTION OF 3D FLUORESCENCE MICROSCOPY IMAGES

Jizhou Li[1]*, Florian Luisier*[2]*, and Thierry Blu*[1]

[1] Department of Electronic Engineering, The Chinese University of Hong Kong, Hong Kong
[2] Roche Diagnostics Hematology, Boston, MA

ABSTRACT

Three-dimensional (3D) deconvolution microscopy is very effective in improving the quality of fluorescence microscopy images. In this work, we present an efficient approach for the deconvolution of 3D fluorescence microscopy images based on the recently developed PURE-LET algorithm. By combining multiple Wiener filtering and wavelet denoising, we parametrize the deconvolution process as a linear combination of elementary functions. Then the Poisson unbiased risk estimate (PURE) is used to obtain the optimal coefficients. The proposed approach is non-iterative and outperforms existing techniques (usually, variants of Richardson-Lucy algorithm) both in terms of computational efficiency and quality. We illustrate its effectiveness on both synthetic and real data.

Index Terms— 3D deconvolution, fluorescence microscopy, Poisson noise, unbiased risk estimate

1. INTRODUCTION

Fluorescence microscopy is widely used in biological research to analyze structures of cells and tissues. Three-dimensional (3D) deconvolution microscopy is a powerful tool to improve the quality of fluorescence microscopy images. It can be applied to several microscopy techniques, for example the conventional wide-field microscopy [1–6], confocal microscopy [7, 8], structured illumination microscopy (SIM) [9, 10], or the localization microscopy [11]. Particularly, in contrast to confocal imaging, wide-field microscopy is more convenient and up to 30% of the total fluorescent light emitted by the specimen can be recorded [12]. Combined with deconvolution techniques, it is very attractive for the observation of subcellular components in living specimens, thus paving the way for a much deeper understanding of the dynamics of biological processes.

Two factors deteriorate the resolution in wide-field fluorescence microscopy. One is blurring, which is caused by the Abbe diffraction limit and modeled by a convolution of the object with a point spread function (PSF). The other one is noise, which further degrades the quality of measured images. In practice, acquisition is performed under low-light conditions when short exposure times are desired to avoid photo-toxicity [13]. In that context, the dominant source of noise follows a Poisson distribution, which is strongly signal-dependent. In order to restore the high resolution image from the blurred and noisy observation, it is important to take this statistics into account. A popular algorithm is Richardson-Lucy (RL) [14–18], which computes a Poisson maximum likelihood estimate. However, this algorithm amplifies noise after a few iterations due to the ill-posedness of inverse convolution. Many authors favor instead the regularization of the Poisson log-likelihood. In this framework, several different regularizers are used such as total-variation [19, 20], wavelet-based [21, 22], and Hessian Schatten-norm based [23]. Unfortunately, the performance improvement of these iterative algorithms comes at the cost of a significant increase of computational burden, which puts a strong limitation on the real application to 3D deconvolution microscopy.

In this work, we extend the PURE-LET approach introduced in [24] to 3D deconvolution microscopy. By combining multiple Wiener filtering and wavelet denoising algorithms, we parametrize the deconvolution process as a linear combination of elementary functions. The Poisson unbiased risk estimate (PURE) is used to optimize these elementary functions in a way that is adapted to the signal-dependent noise statistics. In contrast to existing techniques, the proposed approach is non-iterative and efficient since it essentially amounts to solve a small linear system of equations.

This paper is organized as follows. We firstly discuss the mathematical modeling of the deconvolution problem and our extension of the PURE-LET approach to 3D deconvolution microscopy. Then we compare the proposed method with current state-of-the-art techniques. Finally we present the deconvolution result with one real 3D wide field microscopy image, and compare with the corresponding image from a structured illumination microscope.

2. 3D PURE-LET FOR DECONVOLUTION MICROSCOPY

2.1. Problem statement

Our approach of restoring the underlying true object $\mathrm{x} \in \mathbb{R}_+^N$ from the distorted observation $\mathrm{y} \in \mathbb{R}^N$ is based on the following image-formation model:

$$\mathrm{y} = \alpha\, \mathcal{P}\left(\frac{\mathbf{H}\mathrm{x}}{\alpha}\right)$$

where $N = N_x \times N_y \times N_z$ is the product of the number of pixels along each dimension, $\mathbf{H} : \mathbb{R}^N \to \mathbb{R}^N$ implements a convolution with the PSF "h". We assume that h is normalized to unity. $\mathcal{P}(\cdot)$ represents the effect of Poisson noise and $\alpha \in \mathbb{R}_+$ is a scaling factor, which controls the noise level. Specifically, larger values of α lead to lower intensity images and thus higher Poisson noise.

While the 2D PSF of a wide field microscope can be reasonably well approximated by a Gaussian kernel, no accurate Gaussian approximation exists for 3D PSF [25]. The literature of PSF modeling is extensive, but the most popular one is the Gibson-Lanni model [26]. This model is based on a calculation of the optical path difference between the design conditions and experimental conditions of the objective. It accounts for coverslips and other interfaces between the specimen and the objective. An example of 3D microscopy PSF based on the Gibson-Lanni model is given in Fig. 1.

Our objective is to find an estimate $\hat{\mathrm{x}}$ based on y that is the closest possible to x in the minimum MSE sense. Instead of iteratively estimating $\hat{\mathrm{x}}$ itself, we choose to look for an explicit function $\mathbf{F} : \mathbb{R}^N \to \mathbb{R}^N$ of the measured y such that $\hat{\mathrm{x}} = \mathbf{F}(\mathrm{y})$. That is,

This work was supported by grants from the Research Grants Council (RGC) of Hong Kong (AoE/M-05/12).

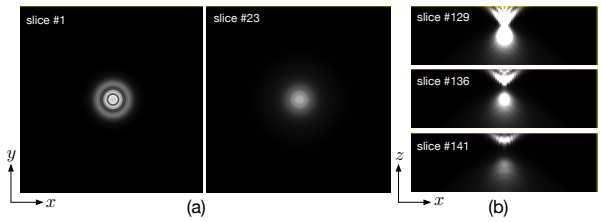

Fig. 1. An example of the 3D microscopy PSF ($256 \times 256 \times 64$) based on the Gibson-Lanni model. (a) (x, y) section in different slices; (b) (x, z) section in different slices. Such non-symmetric patterns occur due to refractive index mismatch between the specimen layer and the immersion layer in the microscope system.

ideally we would like to minimize

$$\mathrm{MSE} = \frac{1}{N}\mathbb{E}\{\|\hat{\mathrm{x}} - \mathrm{x}\|^2\} = \frac{1}{N}\mathbb{E}\left\{\|\mathbf{F}(\mathrm{y}) - \mathrm{x}\|^2\right\}, \qquad (1)$$

where $\mathbb{E}\{\cdot\}$ denotes the mathematical expectation operator.

2.2. The Poisson unbiased risk estimate (PURE)

In practice we do not have access to the oracle MSE between x and the estimate $\hat{\mathrm{x}}$, but we can use an unbiased estimate of its expected value: Poisson unbiased risk estimate (PURE) [24], which solely depends on the observed image y.

$$\mathrm{PURE}\{\mathbf{F}\} = \frac{1}{N}||\mathbf{F}(\mathrm{y})||^2 - \frac{2}{N}\,\mathrm{dif}\,\{\mathbf{H}^{-\mathrm{T}}\mathbf{F}(\mathrm{y})\} + \frac{1}{N}\left(\|\mathrm{y}\|^2 - \alpha\,1^{\mathrm{T}}\mathrm{y}\right) \qquad (2)$$

where $\mathrm{dif}\,\{\mathbf{H}^{-\mathrm{T}}\mathbf{F}(\mathrm{y})\} \stackrel{\mathrm{def}}{=} \sum_{n=1}^{N} y_n \tilde{f}_n(\mathrm{y} - \alpha\,\mathrm{e}_n)$ and $\tilde{\mathbf{F}}(\mathrm{y}) = \mathbf{H}^{-\mathrm{T}}\mathbf{F}(\mathrm{y})$, e_n is the N-dimensional vector with components $\delta_{k-n}, k = 1, 2, ..., N$.

However, there are two implementation issues. One is caused by the possible ill-conditioning of the matrix $\mathbf{H}^{-1}$. This can be addressed by replacing $\mathbf{H}^{-1}$ with the Tikhonov-regularized inverse [1, 27]:

$$\mathbf{H}_\beta^{-1} = \left(\mathbf{H}^{\mathrm{T}}\mathbf{H} + \beta\mathbf{P}^{\mathrm{T}}\mathbf{P}\right)^{-1}\mathbf{H}^{\mathrm{T}},$$

for some parameter $\beta > 0$ and matrix $\mathbf{P} \in \mathbb{R}^N \times \mathbb{R}^N$. In this work, we choose $\mathbf{P}$ to be the discrete Laplacian operator and set $\beta = 1 \times 10^{-5}\alpha\,\mathrm{y}_{\mathrm{mean}}$, where $\mathrm{y}_{\mathrm{mean}}$ is the mean value of y.

The other issue arises from the impractical evaluation of the exact PURE. A direct evaluation of $\mathrm{dif}\,\{\mathbf{H}_\beta^{-\mathrm{T}}\mathbf{F}(\mathrm{y})\}$ would require the calculation of $\mathrm{y}^{\mathrm{T}}\mathbf{H}_\beta^{-\mathrm{T}}\mathbf{F}$ for N perturbed versions of the input y: $(\mathrm{y} - \alpha\,\mathrm{e}_n)$ for $n = 1, ..., N$. Such an evaluation would be computationally unrealistic even with images of reasonable size (e.g. $256 \times 256 \times 128$). Instead, we use the 1st-order derivative to approximate $\mathrm{dif}\,\{\mathbf{H}_\beta^{-\mathrm{T}}\mathbf{F}(\mathrm{y})\}$ given by:

$$\mathrm{dif}\,\{\mathbf{H}_\beta^{-\mathrm{T}}\mathbf{F}(\mathrm{y})\} \simeq \mathrm{y}^{\mathrm{T}}\mathbf{H}_\beta^{-\mathrm{T}}(\mathbf{F}(\mathrm{y}) - \alpha\,\partial\mathbf{F}(\mathrm{y}))$$

where $\partial\mathbf{F}(\mathrm{y}) = [\frac{\partial f_n(\mathrm{y})}{\partial y_n}]_{n=1,...,N}$ is the $N \times 1$ vector made of the first derivative of each function f_n with respect to y_n. Consequently, the PURE unbiased MSE estimate defined in (2) is well approximated by

$$\mathrm{PURE}_{\mathrm{app}}\{\mathbf{F}\} = \frac{1}{N}\|\mathbf{F}(\mathrm{y})\|^2 - \frac{2}{N}\mathrm{y}^{\mathrm{T}}\mathbf{H}_\beta^{-\mathrm{T}}\mathbf{F}(\mathrm{y}) + \frac{2\alpha}{N}\mathrm{y}^{\mathrm{T}}\mathbf{H}_\beta^{-\mathrm{T}}\partial\mathbf{F}(\mathrm{y}) + \frac{1}{N}\left(\|\mathrm{y}\|^2 - \alpha\,1^{\mathrm{T}}\mathrm{y}\right) \qquad (3)$$

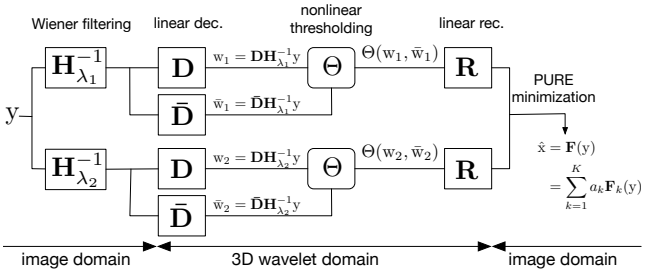

Fig. 2. The flowchart of the proposed PURE-LET algorithm for 3D deconvolution microscopy. The deconvolution process is parametrized as a combination of elementary functions (LET). Each elementary function consists of a Wiener filtering followed by adaptive thresholding in 3D wavelet domain. We then use the PURE (3) to optimize these LETs.

2.3. PURE-LET for 3D Deconvolution Microscopy

In order to find the function $\mathbf{F}$, we describe the deconvolution process $\mathbf{F}$ as a *linear* combination of K (usually) *non-linear* elementary function $\mathbf{F}_k$, termed as linear expansion of thresholds (LET) [27–29]:

$$\mathbf{F}(\mathrm{y}) = \sum_{k=1}^{K} a_k \mathbf{F}_k(\mathrm{y}) \qquad (4)$$

where $K \ll N$ is the number of linear coefficients $\mathrm{a} = [a_k]_{k\in[1,...,K]}$ of the LETs.

Accordingly, the deconvolution problem is reduced to finding the linear coefficients a_k by minimizing the PURE defined in (3). By substituting (4) into (3) and performing differentiation over a_k, this minimization is equivalent to solving the following linear system of equations:

$$\sum_{l=1}^{K} \underbrace{\mathbf{F}_k(\mathrm{y})^{\mathrm{T}}\mathbf{F}_l(\mathrm{y})}_{[\mathbf{M}]_{k,l}} a_l = \underbrace{\mathrm{y}^{\mathrm{T}}\mathbf{H}_\beta^{-\mathrm{T}}\left(\mathbf{F}_k(\mathrm{y}) - \alpha\partial\mathbf{F}_k(\mathrm{y})\right)}_{[\mathrm{c}]_k} \qquad (5)$$

for $k = 1, 2, ..., K$. These equations could be summarized as $\mathbf{M}\mathrm{a} = \mathrm{c}$, where $\mathbf{M} \in \mathbb{R}^{K\times K}$ and $\mathrm{c} = [c_1, ..., c_K]^{\mathrm{T}} \in \mathbb{R}^K$.

We construct the elementary functions $\mathbf{F}_k$'s as basic deconvolution processes (Wiener filtering) followed by denoising (transform-domain thresholding). We use an undecimated filterbank transform in this work (typically, Haar wavelet transform), which has proved to be effective for reducing various types of noise degradations [28–30]. The coefficients provided by the analysis filter are thresholded, and then finally passed to the synthesis filter band. The elementary functions $\mathbf{F}_k$'s consist of multiple Wiener filtering followed by thresholding in the 3D wavelet domain. An illustrative description of the proposed deconvolution approach is shown in Fig. 2. The matrices $\mathbf{H}_{\lambda_k}^{-1} = (\mathbf{H}^{\mathrm{T}}\mathbf{H} + \lambda_k\mathbf{P}^{\mathrm{T}}\mathbf{P})^{-1}\mathbf{H}^{\mathrm{T}}$ represent the Wiener filter with a given regularization parameter λ_k. $\mathbf{D} = [d_{i,j}]_{(i,j)\in[1,...,L]\times[1,...,N]}$ and $\mathbf{R} = [r_{i,j}]_{(i,j)\in[1,...,L]\times[1,...,N]}$ represent a pair of linear decomposition and reconstruction transforms that satisfies the perfect reconstruction condition $\mathbf{RD} = \mathbf{I}$. A linear transformation $\bar{\mathbf{D}} = [\bar{d}_{i,j}]_{(i,j)\in[1,...,L]\times[1,...,N]}$ is applied to the noisy data y in order to yield a coarse estimation of the transform-domain signal-dependent noise variance [29]. Same thresholding functions $\theta_{j,1}$ and $\theta_{j,2}$ as in [24] are used. The 3D wavelet can be constructed as separable products of 1D wavelets by successively applying the analyzing/synthesis filters in three spatial directions

(a) Original (b) Blurred noisy (c) RL-TV (d) ParalIterDecon (e) MitivDecon (f) PURE-LET

Fig. 3. (x, y) and (y, z) sections of the 3D restoration results of the *Bars* image with Poisson noise $\alpha = 0.5$. (a) and (b) The original image and the blurred noisy image, respectively; (c) RL-TV (PSNR=26.92 dB); (d) ParalIterDecon (PSNR = 26.13 dB); (e) MitivDecon (PSNR=26.41 dB); (f) PURE-LET (PSNR=28.26 dB). The computational time of PURE-LET is 38.02s while other approaches need more than 127.05s, see Table 3 for details.

Table 1. PSNRs between the blurred noisy images and the blurred images to indicate the influence of Poisson noise over six representative noise levels.

α	0.25	0.5	1	2	4	8
Bars $256 \times 256 \times 128$	21.31	20.07	18.31	16.10	13.55	10.79
Pollen $2\,56 \times 256 \times 32$	24.36	21.35	18.33	15.33	12.32	9.30

(x, y, z). The deconvolved estimate $\hat{\mathrm{x}}$ can be finally expressed as a function $\mathbf{F}$ of the noisy input signal y as

$$\mathbf{F}(\mathrm{y}) = \sum_{m=1}^{M} \sum_{l=1}^{L} \sum_{j=1}^{J} a_{m,l,j} \underbrace{\mathbf{R}_j \theta_l(\mathrm{w}_{m,j}, \bar{\mathrm{w}}_{m,j})}_{\mathbf{F}_{m,j,k}(\mathrm{y})} + \underbrace{\mathbf{R}_{J+1}\mathbf{D}_{J+1}\mathrm{y}}_{\text{lowpass subband}}$$

where $\mathrm{w}_m = \mathbf{D}\mathbf{H}_{\lambda_m}^{-1}\mathrm{y}, \bar{\mathrm{w}}_m = \bar{\mathbf{D}}\mathbf{H}_{\lambda_m}^{-1}\mathrm{y}$, M is the number of Wiener filters, L is the number of elementary pointwise thresholding functions and J denotes the number of highpass wavelet subbands. As indicated by (5), we have $K = M \times J \times L$ parameters to determine and they are given by the solution of the linear system of equations (5) of order K.

3. EXPERIMENT AND RESULTS

In our approach, we use $M = 2$ Wiener filters with $\lambda_1 = 10^{-3}\alpha\,\mathrm{y}_{\mathrm{mean}}, \lambda_2 = 10^{-2}\alpha\,\mathrm{y}_{\mathrm{mean}}$, where $\mathrm{y}_{\mathrm{mean}}$ is the mean value of y. The decomposition level of 3D undecimated Haar wavelet transform is set to be 2 ($J = 14$). Thus we will have $K = 2 \times 2 \times 14 = 56$ coefficients to be determined via solving (5). Algorithm performance is measured in terms of the peak signal-to-noise ratio (PSNR) in dB, defined as $\mathrm{PSNR} = 10\log_{10}(I_{\max}^2/(\|\hat{\mathrm{x}} - \mathrm{x}\|^2/N))$, where $I_{\max}$ is the maximum intensity of the reference image. All experiments are carried out on a Macbook Pro with a 2.8 GHz Intel Core i7, with 16 GB of RAM. Further images illustrating these results can be found at `http://www.ee.cuhk.edu.hk/~jzli/3D_PURE`.

3.1. Simulation results

We perform experiments over two images, *Bars*[1] and *Pollen*[2]. The synthetic *Bars* image consists of six parallel hollow bars, and the *Pollen* image is a thin optical section through the center of the desiccated stage of the mature pollen showing autofluorescence or harmonic generation of intrinsic structures. The corresponding PSFs with different sizes are generated based on the Gibson-Lanni model [26]. They are used to convolve the ground truth images. The blurred images are subsequently contaminated by Poisson noise with different noise levels (corresponding to different α values). Table 1 presents the PSNRs between the blurred noisy images and the blurred images (as reference), to indicate the influence of Poisson noise over six representative noise levels from $\alpha = 2^{-2}$ to 2^3.

As benchmarks for comparisons, we compare the performance of the PURE-LET algorithm against four state-of-the-art softwares. *R-L* and *RL-TV* represent the classical Richardson-Lucy algorithm [14, 15] and its Total-Variation regularized variant [19], respectively. They are implemented efficiently in the Deconvolu-

[1]The *Bars* image is collected from `http://bigwww.epfl.ch/deconvolution/bars`.

[2]The *Pollen* image is collected from `http://www.cellimagelibrary.org/images/35532`.

Table 2. PSNR comparison with some state-of-the-art algorithms under different noise levels.

α	0.25	0.5	1	2	4	8
Image	*Bars* $256 \times 256 \times 128$					
R-L	27.07	26.90	26.06	26.05	25.06	23.37
RL-TV	27.08	26.92	26.64	26.11	25.38	23.70
ParalIterDecon	26.35	26.13	25.99	25.58	25.38	25.25
MitivDecon	26.48	26.43	26.41	26.30	26.28	26.37
PURE-LET	**28.58**	**28.26**	**27.81**	**27.57**	**27.24**	**27.06**
Image	*Pollen* $256 \times 256 \times 32$					
R-L	28.60	28.03	27.06	25.52	23.21	20.04
RL-TV	28.64	28.13	27.22	25.71	24.80	24.08
ParalIterDecon	25.95	26.11	25.58	24.92	24.01	23.34
MitivDecon	27.55	27.56	27.51	27.47	**26.94**	25.48
PURE-LET	**29.42**	**28.77**	**28.16**	**27.61**	**26.96**	**26.39**

*Best PSNR results within a 0.1 dB margin are highlighted.

Table 3. Comparison of the averaged computational time of various deconvolution algorithms (Units: seconds).

Method	*Bars* $256 \times 256 \times 128$	*Pollen* $256 \times 256 \times 32$
R-L	284.15	62.29
RL-TV	314.23	88.76
ParalIterDecon	257.60	67.39
MitivDecon	125.43	27.29
PURE-LET	36.35	11.01

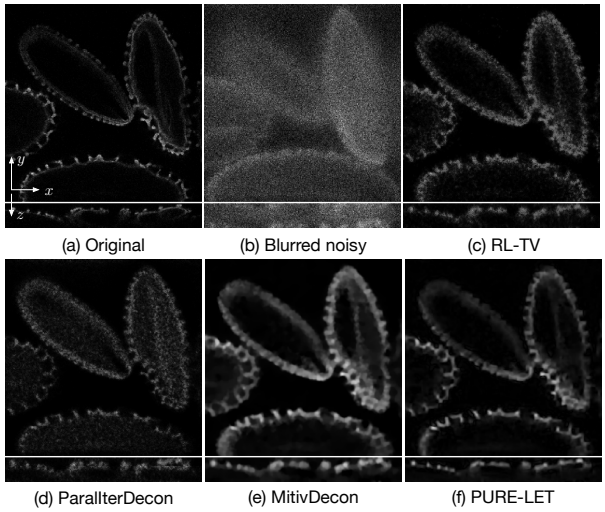

Fig. 4. (x, y) and (x, z) sections of the 3D restoration results of the *Pollen* image with Poisson noise $\alpha = 1$. (a) and (b) The original image and the blurred noisy image, respectively; (c) RL-TV (PSNR=27.22 dB); (d) ParalIterDecon (PSNR = 25.58 dB); (e) MitivDecon (PSNR=27.51 dB); (f) PURE-LET (PSNR=28.16 dB). The computational time of PURE-LET is 11.09s while other approaches need more than 27.52s, see Table 3 for details.

tionLab software[3]. *ParalIterDecon*[4] is an ImageJ plugin for iterative deconvolution. *MitivDecon* [4] is an Icy [31] plugin designed for the restoration of wide field fluorescence microscopy.

Table 2 reports the PSNR comparison results with the ground truth image we have obtained for the various deconvolution methods. This table demonstrates the PURE-LET consistently outperforms other approaches. We would like to stress that our approach is very robust to a wide range of noise levels. Fig. 3 and Fig. 4 show the comparison of visual quality of *Bars* and *Pollen* images in sections. Our method can preserve more image details with limited artifacts.

Table 3 reports the computational time of various deconvolution methods. It can be seen that our approach is significantly faster than other approaches. For instance, our algorithm is roughly 9 times faster than the commonly used *RL-TV* algorithm for the *Bars* image with size $256 \times 256 \times 128$. Importantly, the PURE-LET computational time is achieved using only a direct Matlab implementation (no mex files), which contrasts with the Java optimized code of other algorithms.

3.2. Real image result

We use the image of microtubules in a Drosophila S2 cell[5]. Cells were chemically fixed, and labeled with an anti-tubulin primary antibody and an Alexa Fluor 488 secondary antibody. This dataset is collected on a Zeiss Elyra structured illumination microscope (SIM). It consists of one 3D wide field image and a super-resolution SIM image which can be used for comparison. We cropped and rescaled these images to highlight the main structures. These images are of size $256 \times 256 \times 44$. The pixel size is then $0.1588\ \mu$m.

[3]The DeconvolutionLab software is available at `http://bigwww.epfl.ch/deconvolution/deconvolutionlab1`.

[4]The *ParalIterDecon* is available at `http://imagej.net/Parallel_Iterative_Deconvolution`.

[5]`http://www.cellimagelibrary.org/images/36797`.

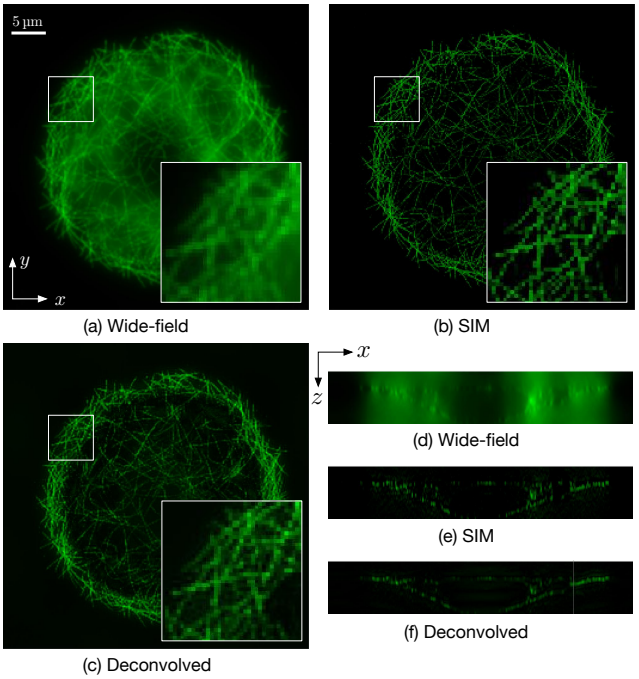

Fig. 5. Comparison of the deconvolution result and the super-resolution SIM image on the real data. (a-c) (x, y) section; (d-f) (x, z) section. (a) and (d) the measured wide field image; (b) and (e) the super-resolution image given by the SIM technique; (c) and (f) the deconvolved image obtained by the PURE-LET approach (computation time: 21.48 seconds).

We manually tuned the parameters of the Gibson-Lanni model in order to estimate the PSF and the noise factor α. The deconvolution result and the comparison with the SIM image are shown in Fig. 5. Compared with the wide field image, the deconvolved image produces a much better quality image, in particular increases the image resolution along the axial direction. Note that SIM is known to produce a two-fold increase of the resolution compared with that of the wide field image [32]. Our approach can achieve roughly the same resolution, but with a much faster acquisition time: the SIM technique needs 15 wide field images (with different illuminations) to reconstruct one super-resolution image [32] while our deconvolution approach needs to process just one wide field image.

4. CONCLUSION

We proposed a non-iterative and efficient deconvolution approach for 3D fluorescence microscopy images. The deconvolution process is linearly parametrized as a combination of few elementary functions (LET). By considering the Poisson noise statistics in the fluorescence microscopy images, we use a statistical estimate of the MSE (PURE) to optimize these LETs. The proposed PURE-LET approach outperforms current state-of-the-art techniques, both qualitatively and computationally. We expect to further improve its performance by using more decomposition levels or more sophisticated transforms. In addition, the result on real wide field image shows the potential of deconvolution techniques to achieve the super-resolution of Structured Illumination Microscopy. Future work will focus on estimating the PSF automatically from the measurements.

5. REFERENCES

[1] P. Sarder and A. Nehorai, "Deconvolution methods for 3-D fluorescence microscopy images," *IEEE Signal Process. Mag.*, vol. 23, no. 3, pp. 32–45, 2006.

[2] A. Griffa, N. Garin, and D. Sage, "Comparison of deconvolution software in 3D microscopy: A user point of viewpart 1," *GIT Imag. & Microsc.*, vol. 12, no. EPFL-ARTICLE-163617, pp. 43–45, 2010.

[3] T. Kenig, Z. Kam, and A. Feuer, "Blind image deconvolution using machine learning for three-dimensional microscopy," *IEEE Trans. Pattern Anal. Mach. Intell.*, vol. 32, no. 12, pp. 2191–2204, 2010.

[4] F. Soulez, "A "learn 2D, apply 3D" method for 3D deconvolution microscopy," in *Proc. IEEE Int. Symp. Biomed. Imaging (ISBI)*, Beijing, China, 2014, pp. 1075–1078.

[5] B. Kim and T. Naemura, "Blind depth-variant deconvolution of 3d data in wide-field fluorescence microscopy," *Sci. Rep.*, vol. 5, no. 9894, pp. 1–9, 2015.

[6] C. Kervrann, C. O. Sanchez Sorzano, S. T. Acton, J. C. Olivo Marin, and M. Unser, "A guided tour of selected image processing and analysis methods for fluorescence and electron microscopy," *IEEE J. Sel. Topics Signal Process.*, vol. 10, no. 1, pp. 6–30, 2016.

[7] P. Pankajakshan, B. Zhang, L. Blanc-Féraud, Z. Kam, J.-C. Olivo-Marin, and J. Zerubia, "Blind deconvolution for thin-layered confocal imaging," *Appl. Opt.*, vol. 48, no. 22, pp. 4437–4448, 2009.

[8] R. Zanella, G. Zanghirati, R. Cavicchioli, L. Zanni, P. Boccacci, M. Bertero, and G. Vicidomini, "Towards real-time image deconvolution: application to confocal and STED microscopy," *Sci. Rep.*, vol. 3, no. 2523, pp. 1–8, 2013.

[9] F. Orieux, E. Sepulveda, V. Loriette, B. Dubertret, and J.-C. Olivo-Marin, "Bayesian estimation for optimized structured illumination microscopy," *IEEE Trans. Image Process.*, vol. 21, no. 2, pp. 601–614, 2012.

[10] N. Chakrova, B. Rieger, and S. Stallinga, "Deconvolution methods for structured illumination microscopy," *J. Opt. Soc. Am. A*, vol. 33, no. 7, pp. B12–B20, 2016.

[11] E. A. Mukamel, H. Babcock, and X. Zhuang, "Statistical deconvolution for superresolution fluorescence microscopy," *Biophys. J.*, vol. 102, no. 10, pp. 2391–2400, 2012.

[12] P. Shaw, "Comparison of widefield/deconvolution and confocal microscopy for three-dimensional imaging," in *Handbook of Biological Confocal Microscopy*, J. Pawley, Ed. New York: Springer, 2006, pp. 453–467.

[13] M. Arigovindan, J. C. Fung, D. Elnatan, V. Mennella, Y.-H. M. Chan, M. Pollard, E. Branlund, J. W. Sedat, and D. A. Agard, "High-resolution restoration of 3D structures from widefield images with extreme low signal-to-noise-ratio," *Proc. Natl. Acad. Sci. U.S.A.*, vol. 110, no. 43, pp. 17 344–17 349, 2013.

[14] W. H. Richardson, "Bayesian-based iterative method of image restoration," *J. Opt. Soc. Am. A*, vol. 62, no. 1, pp. 55–59, 1972.

[15] L. B. Lucy, "An iterative technique for the rectification of observed distributions," *The Astron. J.*, vol. 79, p. 745, 1974.

[16] M. A. Bruce and M. J. Butte, "Real-time gpu-based 3d deconvolution," *Opt. Express*, vol. 21, no. 4, pp. 4766–4773, 2013.

[17] H. Wang and P. C. Miller, "Scaled heavy-ball acceleration of the richardson-lucy algorithm for 3D microscopy image restoration," *IEEE Trans. Image Process.*, vol. 23, no. 2, pp. 848–854, 2014.

[18] M. Ponti, E. S. Helou, P. J. S. Ferreira, and N. D. Mascarenhas, "Image restoration using gradient iteration and constraints for band extrapolation," *IEEE J. Sel. Topics Signal Process.*, vol. 10, no. 1, pp. 71–80, 2016.

[19] N. Dey, L. Blanc-Feraud, C. Zimmer, P. Roux, Z. Kam, J.-C. Olivo-Marin, and J. Zerubia, "Richardson–Lucy algorithm with total variation regularization for 3D confocal microscope deconvolution," *Microsc. Res. Tech.*, vol. 69, no. 4, pp. 260–266, 2006.

[20] Z. T. Harmany, R. F. Marcia, and R. M. Willett, "This is SPIRAL-TAP: Sparse Poisson intensity reconstruction algorithms: theory and practice," *IEEE Trans. Image Process.*, vol. 21, no. 3, pp. 1084–1096, 2012.

[21] C. Vonesch and M. Unser, "A fast multilevel algorithm for wavelet-regularized image restoration," *IEEE Trans. Image Process.*, vol. 18, no. 3, pp. 509–523, 2009.

[22] M. Carlavan and L. Blanc-Feraud, "Sparse Poisson noisy image deblurring," *IEEE Trans. Image Process.*, vol. 21, no. 4, pp. 1834–1846, 2012.

[23] S. Lefkimmiatis and M. Unser, "Poisson image reconstruction with Hessian Schatten-Norm regularization," *IEEE Trans. Image Process.*, vol. 22, no. 11, pp. 4314–4327, 2013.

[24] J. Li, F. Luisier, and T. Blu, "Deconvolution of Poissonian images with the PURE-LET approach," in *Proc. IEEE Int. Conf. Img. Proc. (ICIP)*, Phoenix, USA, 2016, pp. 2708–2712.

[25] B. Zhang, J. Zerubia, and J.-C. Olivo-Marin, "Gaussian approximations of fluorescence microscope point-spread function models," *Appl. Opt.*, vol. 46, no. 10, pp. 1819–1829, 2007.

[26] S. F. Gibson and F. Lanni, "Experimental test of an analytical model of aberration in an oil-immersion objective lens used in three-dimensional light microscopy," *J. Opt. Soc. Am. A*, vol. 9, no. 1, pp. 154–166, 1992.

[27] F. Xue, F. Luisier, and T. Blu, "Multi-Wiener SURE-LET deconvolution," *IEEE Trans. Image Process.*, vol. 22, no. 5, pp. 1954–1968, 2013.

[28] T. Blu and F. Luisier, "The SURE-LET Approach to Image Denoising," *IEEE Trans. Image Process.*, vol. 16, no. 11, pp. 2778–2786, 2007.

[29] F. Luisier, T. Blu, and M. Unser, "Image denoising in mixed Poisson-Gaussian noise," *IEEE Trans. Image Process.*, vol. 20, no. 3, pp. 696–708, 2011.

[30] J. L. Starck, J. Fadili, and F. Murtagh, "The undecimated wavelet decomposition and its reconstruction," *IEEE Trans. Image Process.*, vol. 16, no. 2, pp. 297–309, 2007.

[31] F. De Chaumont, S. Dallongeville, N. Chenouard, N. Hervé, S. Pop, T. Provoost, V. Meas-Yedid, P. Pankajakshan, T. Lecomte, Y. Le Montagner *et al.*, "Icy: an open bioimage informatics platform for extended reproducible research," *Nat. Methods*, vol. 9, no. 7, pp. 690–696, 2012.

[32] M. G. Gustafsson, L. Shao, P. M. Carlton, C. R. Wang, I. N. Golubovskaya, W. Z. Cande, D. A. Agard, and J. W. Sedat, "Three-dimensional resolution doubling in wide-field fluorescence microscopy by structured illumination," *Biophys. J.*, vol. 94, no. 12, pp. 4957–4970, 2008.